Estimating dry bed periods in non-perennial rivers using Sentinel-2 satellite data

Journal of Hydrology 660 (2025) 133416

Contents lists available at ScienceDirect

Journal of Hydrology

journal homepage: www.elsevier.com/locate/jhydrol

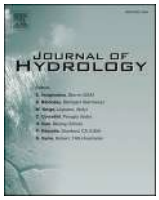

Estimating dry bed periods in non-perennial rivers using Sentinel-2 satellite data

Carmela Cavallo [a,*], Luca Sarno [a], Maria Nicolina Papa [a], Giovanni Negro [b], Paolo Vezza [b], Giuseppe Ruello [c], Massimiliano Gargiulo [d]

[a] Department of Civil Engineering, University of Salerno, 84084 Fisciano, SA, Italy
[b] Department of Environment, Land and Infrastructure Engineering, Polytechnic University of Torino 10129 Torino, Italy
[c] Department of Information Technology and Electrical Engineering, University of Napoli "Federico II", 80125 Napoli, Italy
[d] CIRA, Italian Aerospace Research Centre, 81043 Capua, Caserta, Italy

ARTICLE INFO

Keywords:
Non-perennial rivers
Satellite data
Sentinel-2 imagery
Continuous monitoring
Climate change, Duration of dry period

ABSTRACT

Information on the number of dry bed reaches along non-perennial rivers is still lacking, as well as the duration of their non-flow periods. Measurements at conventional gauging stations are not exhaustive due to the high spatial variation of flow rate values and water presence along the non-perennial river network. The availability of moderate-resolution multispectral satellite data from the Sentinel-2 mission offers an unprecedented opportunity to monitor water presence on a broad scale. In this study, we developed a new, automatic approach to detect water, sediments and vegetation along non-perennial rivers by Sentinel-2 satellite imagery. Specifically, we implemented a classification method based on the minimum spectral distance between single pixel's reflectance and reference spectral signatures, previously obtained from reference images. The classification results are, then, compared with very high-resolution images (resolution of 0.5 m or smaller) acquired by unmanned aerial vehicle and from Google Earth Pro. The performance (F1-score = 0.7) is significantly higher than the ones obtained with the classic algorithm based on the thresholding of Normalized Difference Water Index (F1-score = 0.5). Exploiting the proposed method, we estimated the duration of dry bed condition over two reaches of the Mingardo River (South Italy), from 2017 to 2022. The duration of the dry bed condition resulted to be significantly variable from year to year with the longest and the shortest dry periods respectively, in summer 2017 and in summer 2022. The study demonstrates the feasibility and robustness of using moderate-resolution multispectral images for large-scale monitoring of non-perennial rivers in a cost-effective way.

1. Introduction

Non-perennial rivers (NPRs) are characterized by surface water flow discontinuous in space and/or in time. Based on the duration of water presence in the riverbed, non-perennial rivers are distinguished into "intermittent" and "ephemeral", i.e. channel flowing seasonally for 3 months or more and channel flowing only temporarily in response to rainfall inputs (Zimmer and McGlynn, 2017). These rivers typically exhibit three different flow conditions: (i) the "flowing" condition characterized by a continuous surface flow, (ii) the "dry" condition in which the riverbed is completely without surface water, and (iii) the "ponding" condition characterized by ponds or pools of water that are not connected to each other. NPRs, due to the coexistence of terrestrial and aquatic ecosystems, shelter specific freshwater biodiversity and play a crucial role in biogeochemical cycles (Datry et al. 2014). These rivers are widespread globally, and it is predicted that an increasing portion of the river network will stop flowing continuously in the coming decades due to climate change (e.g., Messager et al. 2021; Shanafield et al. 2021). The extreme recorded drought that hit Europe in the summer 2022 (Toreti et al. 2022a, 2022b; Faranda et al., 2023) affected substantially the availability and quality of water in fluvial environments: several perennial rivers stopped flowing and many others reached historically low levels. The effects of climate change on river environments are further amplified by longer dry seasons and higher temperatures, which in turn increases the demand of irrigation water. The European Commission has long called on Member States to develop monitoring systems and actions to counter the effects of climate change on fluvial systems (EC, 2009a,b), which are to be implemented in the Water

* Corresponding author.
E-mail address: ccavallo@unisa.it (C. Cavallo).

https://doi.org/10.1016/j.jhydrol.2025.133416
Received 4 November 2023; Received in revised form 29 September 2024; Accepted 27 April 2025
Available online 2 May 2025

Framework Directive (WFD), the Floods Directive and the European Union Strategy on Water Scarcity and Droughts (De Girolamo et al., 2017; Commission of the European Communities., 2009). However, to date a statutory system providing adequate guidance on the identification, classification management and protection of non-perennial rivers and streams is still lacking. This crucial deficiency is mainly due to the lack of knowledge about the position and length of the non-perennial reaches in the river network, and the lack of information on the duration of water presence. Traditional gauging stations are unable to provide detailed information on the spatial distribution and duration of water presence. Zimmer et al. (2020) reported that traditional gauging stations may produce a zero-flow reading, also in flowing conditions, when the water does not pass through the monitored point. Additionally, Cavallo et al. (2022b) clearly showed that point measurements, are unable to distinguish the ponding phase from the dry one and, in some cases, not even the flowing condition from the non-flowing one. In this regard, the use of satellite data provides a cost-effective solution to monitor the water presence along the river network (Di Ciacca et al. 2023).

Remote sensing data have been successfully used to monitor the water surface along perennial rivers (Carbonneau et al. 2020; Cavallo et al. 2021). Only more recently, few researches have focused on the use of these data for monitoring non-perennial rivers (Cavallo et al., 2022; Gao et al., 2021; Maswanganye et al., 2022a,b; Seaton et al., 2020; Wang and Vivoni, 2022). The usual dichotomy between spatial resolution and acquisition frequency is particularly relevant for this application, especially due to the small extension of wet channels and ponds and the high variability of flowing condition over time. For example, the very high spatial resolution images (VHR, resolution below 0.50 m) from commercial satellites (World-View, GeoEye) allows detecting small areas of water but the high acquisition costs, and in some cases the low frequency of the acquisitions, strongly limit their usage. Conversely, high temporal resolution satellite datasets, such as MODIS (with a one-day time resolution) with coarse spatial resolution are not suitable for identifying narrow wet channels and water ponds. The Landsat program, born by the joint effort of the United States Geological Survey (USGS) and the National Aeronautics and Space Administration (NASA), provides the most extended temporal series of the Earth's land observations from satellites, from 1972 up to now. The extended observation period is useful for long-term analysis, but its coarse resolution (30 m) severely limits its use for non-perennial rivers. Thanks to a spatial resolution of 10 m and an acquisition frequency of ≈5 days, multispectral satellite data from the Copernicus Sentinel-2 (S2) mission of the European Space Agency (ESA) constitute a suitable trade-off point. S2 data are available free of charge, which greatly encourages their use by researchers, public agencies and technicians. Seaton et al. (2020) examined the suitability of various multispectral indices derived from Sentinel-2 and Landsat-8 satellite imagery for identifying and mapping water surface areas along three non-perennial rivers (Nuwejaars, Breede and Tankwa Rivers) located in the Western Cape of South Africa. Gao et al. (2021) extracted Dynamic Surface Water Estimate (DSWE) from Landsat data in high-order streams and compared them with simulated streamflow, obtained by Coupled Routing and Excess STorage (CREST) model. Maswanganye et al. (2022a) explored the use of multi-source satellite data (Sentinel-1, synthetic aperture radar data, and Sentinel-2) to identify and monitor the spatial distribution of pools along two non-perennial rivers, Touws and Molototsi Rivers, located in South Africa. The authors extracted water surfaces from S2 data, using three multispectral indices, including the Normalized Difference Water Index (NDWI, Mcfeeters, 1996), the Modified Normalized Difference Water Index (MNDWI, Xu, 2006), the Normalized Difference Vegetation Index (NDVI, Curran 1983), and a supervised Random Forest classification method. They also extracted water surfaces from the Sentinel-1 SAR data with a threshold classification method. Overall, these studies reported similar results, indicating that multispectral indices derived from Sentinel-2 imagery outperform those from Landsat-8 for identifying water surfaces. Among the various indices, the NDWI and the Automated Water Extraction Index for Shadowed (AWEIsh) by (Feyisa et al., 2014) demonstrated the best performance in mapping water surfaces. NDWI showed the highest accuracy, being able to classify pools larger than 400 km2, while MNDWI yielded lower performance likely because it uses the short-wave infrared (SWIR) band, which is acquired at a lower resolution than the bands used by the NDWI. More recently, Maswanganye et al. (2022b) explored the use of remotely sensed data for the water balance analysis of the pools along the Touws River. The authors exploited the MNDWI, extracted from S2 images, to map water surfaces and used other satellite data sources (MODIS 16) to get estimations of evapotranspiration data. Wang and Vivoni (2022) employed the Planet Scope images, acquired by the CubeSat constellation, and exploited the lower reflectance of water, compared to other types of land cover, in the near infrared (NIR) band to identify whether a reach is ephemeral or intermittent. Cavallo et al. (2022b) systematically investigated the S2 reflectance of various land cover classes across three river reaches of the Cilento National Park (Southern Italy), and identified a false colour composition (SWIR, NIR, and RED) capable of making water surfaces distinguishable from other river corridors' land covers. Yet, an algorithm to automatically identify the different flow statuses is currently lacking.

To overcome this gap, this paper proposes an automatic classification method on S2 images to identify and monitor water, sediments and vegetation surfaces and estimate the duration of dry period in non-perennial rivers. The proposed automatic classification method is based on the minimum distance between the reflectance of a single pixel for all S2 bands (provided with 10 and 20 m resolutions) and the reference spectral signature of land cover classes. Reference spectral signatures have been previously extracted by overlaying simultaneous acquisitions of S2 and very high spatial resolution images, from which land cover classes could be easily identified manually. The method is tested over two reaches of the Mingardo River (South Italy).

2. The study site

The case studies are two reaches of the Mingardo River in the Mediterranean region. The Mingardo River is in the Cilento National Park, located in the province of Salerno (Southern Italy). The river has a total length of about 38 km and a catchment of about 232 km^2. It originates from a spring located at an altitude of 1′041 m a.s.l. on the Gelbison Mountain and flows to the Tyrrhenian Sea close to Palinuro village. The climate is characterized by a wet season from mid-September to May and by a warm season from June to mid-September. Typically, rainfall gradually increases from late September (or early October), peaks in November, and decreases in early May. Consequently, the river is characterized by a strong flow decrease during the summer season, when the downstream reaches, which are the subject of this study, are usually dry. In detail, the study focuses on two lowland reaches named M1 and M2 (see Fig. 1). They are approximately 4 km and 2 km long and with an average width of the active channel of approximately 62 m and 117 m, respectively. The reaches under study have a sandy-gravel bed, M1 is confined (C) with a sinuous (S) active channel (C-S) and M2 is partly confined (PC) with a wandering (W) morphology (PC-W, following the approach proposed by Gurnell et al., 2016). A hydrometric station is located approximately 500 m downstream of the end of reach M2, where the water level fluctuated between 2.31 m and 4.61 m during the years 2017–2022.

3. Remote sensing data and methods

3.1. Sentinel-2 and high-resolution images

The S2 mission is part of the Copernicus Earth Observation program led by the European Commission (EC) and operated by the European Space Agency (ESA). The S2 mission provides multispectral images from

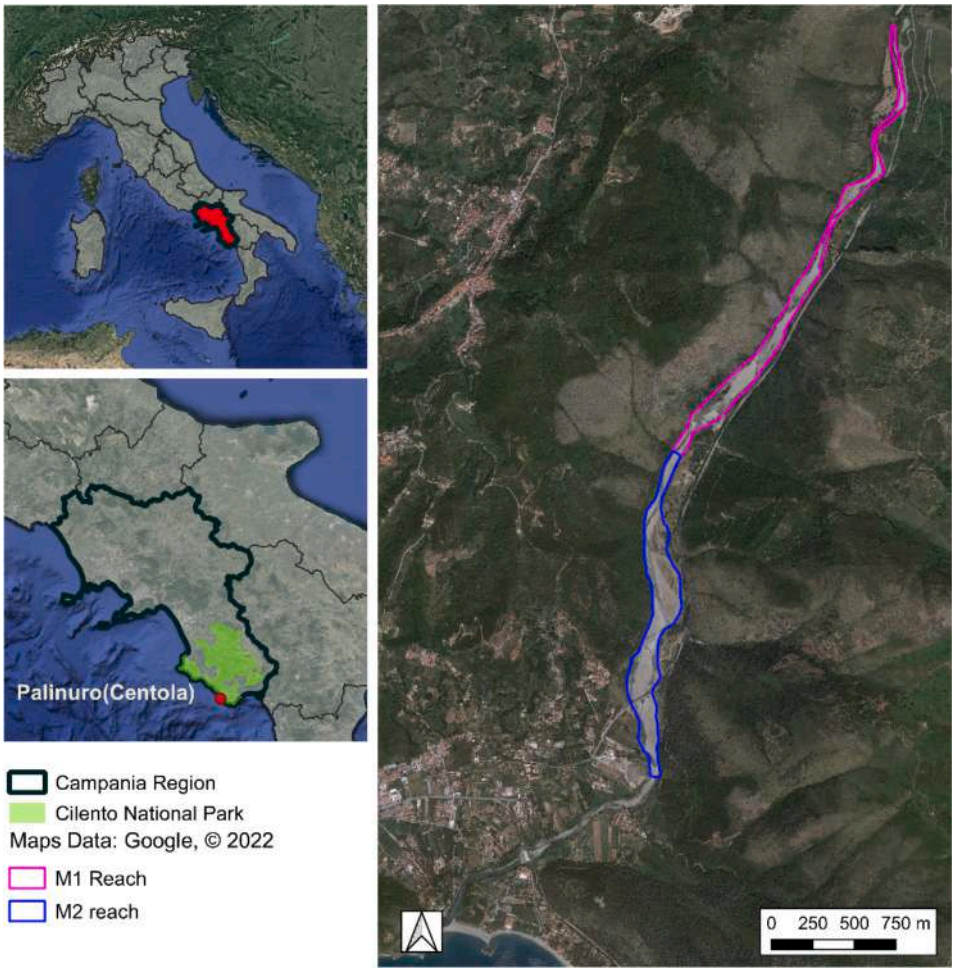

Fig. 1. The study area on the Mingardo River. The two reaches, named M1 and M2, are located in the Cilento National Park, Campania Region, Italy.

a constellation of twin satellites in the same orbit: Sentinel-2A (S2A), launched on the 23rd June 2015 and Sentinel-2B (S2B), launched on the 7th March 2017. Both satellites are equipped with a multi-spectral instrument (MSI) and provide under cloud-free conditions moderate resolution images with 5-day revisit time from March 2017. Please note that, prior to the launch of the second satellite (S2B), the revisit time was 10 days. The MSI provides 13 spectral bands with variable spatial resolution. In this work, we used both 10 m and 20 m resolution bands: B2, B3, B4 in the visible and B8 in the near-infrared with spatial resolution 10 m; B5, B6 e B7 in the Red-Edge, B8a in the NIR narrow and B11 and B12 in the short-wave infrared with spatial resolution of 20 m. The S2 collection delivers Top-of-Atmosphere (TOA) reflectance (level-1C) products and Bottom-of-Atmosphere (BOA) reflectance images (level-2A).

As a ground truth reference we used two VHR images (resolution of 0.5 m) acquired on 13th December 2021 and on 11th July 2022 by Unmanned Aerial Vehicle (UAV), geo-located pictures acquired on 6th February 2021 and a VHR satellite image (resolution less than 1 m), acquired on 14th June 2019 and obtained from Google Earth Pro.

Table 1
Sentinel-2 satellite acquisitions and images used as reference.

Images used as reference	Sentinel-2 satellite images
11 July 2022 (UAV)	11 July 2022
13 December 2021 (UAV)	13 December 2021
6 February 2021 (geo-located pictures)	6 February 2021
14 June 2019 (Google Earth Pro)	12 June 2019

Table 1 reports the ground truth images and the S2 acquisition closest in time.

It is worth noting that all the ground truth images were acquired on the same day of the S2 images, exception made for the Google Earth Pro image that was captured two days after the S2 one.

3.2. Automatic classification method

The amount of energy that an object reflects and emits over a wide range of wavelengths is called the spectral response pattern, also known as the spectral signature. Since soils, water, and vegetation reflect various wavelengths of the electromagnetic spectrum in different ways, the shape of the spectral signature allows for distinguishing different types of land cover (Ma et al., 2019). In this work, we implemented an automatic tool for the classification of five land covers classes: (i) deep water (deeper than ≈1m), (ii) shallow water, (iii) sediments, (iv) grass and (v) dense vegetation such as bushes and trees. The procedure consists of two steps. Firstly, we applied a threshold method, based on NDVI, to distinguish the dense vegetation class. Next, we used a minimum distance classification method (MD) to distinguish the other classes. The MD method consist in computing the difference between the spectral signature ($\boldsymbol{x}$) of the pixel and the reference spectral signature ($\boldsymbol{y}$) of each of the land cover classes. Both $\boldsymbol{x}$ and $\boldsymbol{y}$ are vectors of n dimension (with $n = 10$) containing the reflectance in the selected S2 bands. The pixel is then assigned to the class that yields the minimum Euclidean distance d($\boldsymbol{x}$,$\boldsymbol{y}$) between $\boldsymbol{x}$ and $\boldsymbol{y}$:

$$d(\boldsymbol{x},\boldsymbol{y}) = \sqrt{\sum_{i=1}^{n} (\boldsymbol{x}_i - \boldsymbol{y}_i)^2} \quad (1)$$

The smallest $d(\boldsymbol{x},\boldsymbol{y})$ value is estimated by discriminant criterion (Richards and Jia, 2006):

$$\boldsymbol{x} \in C_K \leftrightarrow \; d(\boldsymbol{x}, \boldsymbol{y}_k) < d(\boldsymbol{x}, \boldsymbol{y}_j) \forall k \neq j \quad (2)$$

where C_k is the land cover class k, and $\boldsymbol{y}_k$ and $\boldsymbol{y}_j$ are the spectral signatures of class k and j, respectively.

The signatures $\boldsymbol{y}$ were extracted as follow. On the basis of the ground truths introduced in Sect. 3.1, we drew 30 polygons (with a total area of approx. 0.3 km^2) that identify areas with homogeneous covers. For VHR images, the polygons were drawn with GIS tools after visual inspection (see Fig. 2a). The capability of distinguishing deep and shallow water was made possible only for the UAV derived orthophoto. For geolocated ground photos, the polygons were drawn through the visual inspection of the FCI image, obtained with the technique proposed by Cavallo et al. (2022b), after locating the position of the photos on the image (see Fig. 2b).

The spectral signature ($\boldsymbol{y}$) was then obtained by calculating, for each band, the average of the reflectance of curves corresponding to the pixels of the S2 images that are contained in the polygons. This operation was performed trough Google Earth Engine (GEE), a free geospatial processing service provided by Google Cloud Platform.

We used the spectral signatures extracted by the acquisitions of June 2019 and December 2021 as reference for the implementation of the MD algorithm, and the polygons extracted by the acquisitions of February 2022 and July 2022 for the validation. Fig. 3 shows the workflow of the proposed method.

Once obtained the pixel level semantic segmentation, we count the number of water pixels for each available S2 date within the active channel to estimate the dry duration. The river is defined dry when no water pixel is found in the active channel. If, conversely, any water pixel is detected within the active channel, it can be inferred that the reach is in the flowing or ponding phase (wet phases). For the calculation of the time intervals (in terms of days) corresponding to wet and dry phases, unaltered flow conditions are assumed between two consecutive acquisitions. Conversely, a nearest neighbor interpolation between consecutive images exhibiting different flow status is performed in order to estimate the dry bed duration on a daily basis. We observed that in some years the dry period lasted until October. Hence, from the year 2017/2018 we chose to study the dry bed duration in the yearly time interval starting from 1st November to 31st October. In order to avoid too coarse time resolutions, the months prior to the launch of the Sentinel-2B satellite (i.e., before March 2017) were not considered. Therefore, for the year 2017 only, we considered the shorter time period from 1st March to 31st October. It is worth underlining that the water masks extracted from Sentinel-2 were obtained with an average revisit time of ≈15 days during the wet season and ≈10 days during the dry season.

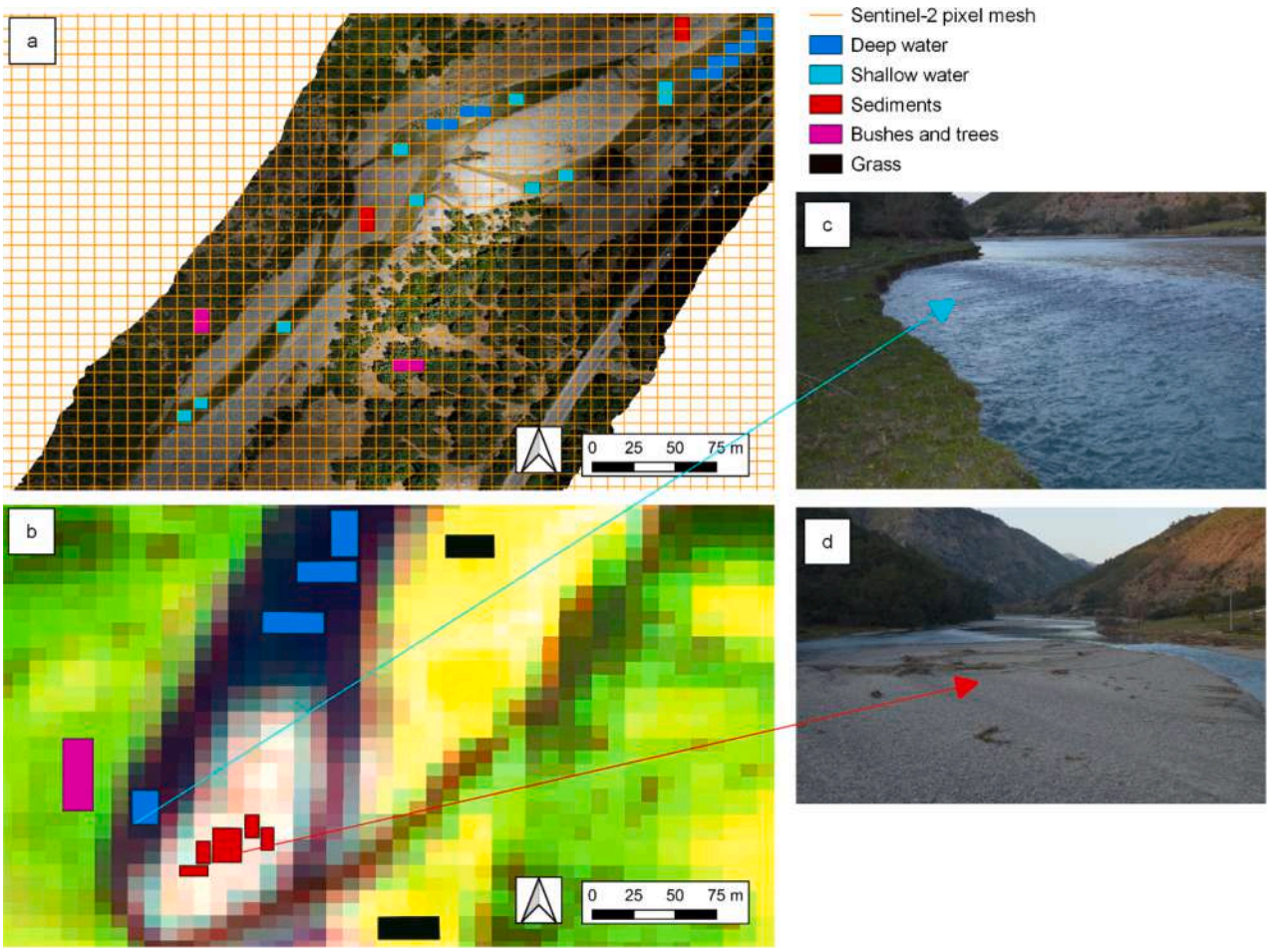

Fig. 2. (a) Patch of the image acquired by UAV on 11 July 2022 overlapped with the Sentinel-2 pixel mesh and representative polygons of the various land cover classes (bushes and trees, water and sediments), (b) FCI of the Sentinel-2 image of 6 February 2021 and representative polygons of the various classes (bushes and trees, grass, water and sediments); (c, d) geolocated images.

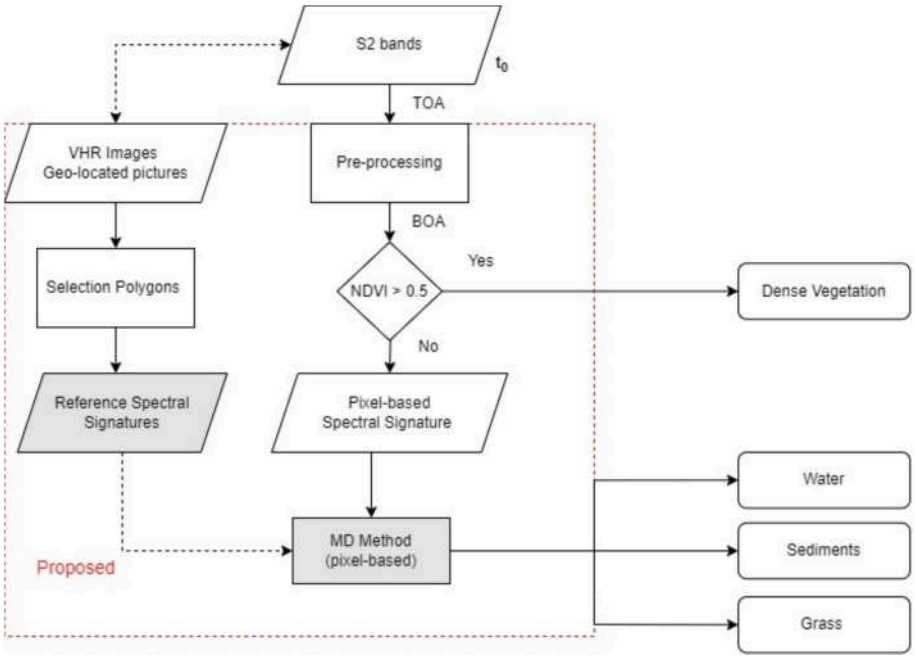

Fig. 3. Workflow of the proposed method.

3.3. Accuracy assessment

The quality of the results are assessed from visual and quantitative standpoints. In the visual inspection, we compared the result of the MD and the NDWI-based method, showing them together with the FCI previously proposed by Cavallo et al. (2022b). Then, in numerical comparison we used some common metrics, classically employed in segmentation and classification problems, such as Overall Accuracy, Precision, Recall, and F1-score (Goutte et al., 2005):

$$Accuracy = \frac{TP + TN}{\mathrm{TP} + \mathrm{FP} + \mathrm{FN} + \mathrm{TN}} \tag{3}$$

$$Precision = \frac{TP}{\mathrm{TP} + \mathrm{FP}} \tag{4}$$

$$Recall = \frac{TP}{\mathrm{TP} + \mathrm{FN}} \tag{5}$$

$$F_1 score = 2^{*}\frac{Precision^{*}Recall}{\mathrm{Precision} + \mathrm{Recall}} \tag{6}$$

where *TP*, *TN*, *FP*, and *FN* are the number of true positives, true negatives, false positives, and false negatives, respectively. Ideally speaking, if *FP* and *FN* are equal to zero, accuracy, precision, recall, and F1 score are equal to 1.

In particular, we performed two quantitative assessments, hereafter named as Test 1 and Test 2. For Test 1, the classification of land cover obtained by the MD method and the classification obtained manually (ground truth) by drawings polygons for each land cover class, as described in Sect. 3, are compared in terms of the abovementioned metrics. In particular, for this test, we used polygons extracted from the acquisitions of the July 2022 and of the February 2021, which were not used for the definition of the reference spectral signatures. Test 2 compares the water detection obtained using the MD method and the NDWI-based with the wet channel drawn on the VHR images reported in Table 1. It should be noted that Test 1 is confined to the pixels contained in the polygons (30 pixels for each land cover class) while Test 2 is applied to the entire image.

4. Results

4.1. Spectral signatures

Fig. 4 shows the spectral signatures of the land-cover classes computed on S2 bands, simultaneous to the ground truth data listed in Table 1.

The reflectance values of the vegetation classes vary depending on several factors, such as type of vegetation, density, growth state, moisture content and leaf structure. This explained why the reflectance values of the vegetation in the near-infrared wavelengths are significantly higher in summer (cf. Fig. 4a and 4d) than in winter (cf. Fig. 4b and 4c), as previously observed by Ferreira and Huete (2004). The spectral signatures of sediments class show similar reflectance values in the various acquisitions, except for December 2021 (Fig. 4c) where the curve is slightly lower than for the other acquisitions.

This variability could be due to the higher water content of December 2021 as, the reflectance of wet sediments is known to be lower at all wavelengths (Ishida et al., 1991). This explanation is corroborated by the duration of the dry period before the June (Fig. 4a), February (Fig. 4b), December (Fig. 4c) and July (Fig. 4d) acquisitions, which are equal to 10, 4, 1 and 3 days, respectively. However, it is interesting to note that, although the reflectance values of vegetation and sediments show a degree of seasonality, the shapes of the spectral signatures are independent from the season. In fact, it is systematically observed that the spectral signature of vegetation (both for the case of bushes/trees and grass) has high reflectance values in the NIR wavelengths and lower values in the visible and SWIR wavelengths. This finding suggested that even a simple NDVI-based threshold classification method can be efficiently used to roughly distinguish vegetated from non-vegetated areas (Curran, 1983). For this reason, we chose to employ a simple threshold method based on NDVI to identify the dense vegetation (bushes and trees), with a threshold of 0.5, similar to what was done for example by Holben 1986 and Rutkay et al. (2020). In this way, we removed the dense vegetation pixels from the following analysis, and we applied the MD algorithm on the remaining pixels to identify the other three classes (grass, sediment and water).

The shape of the spectral signature for water varies with the depth. In the presence of deep water ($h > \approx 1m$), infrared wavelengths are totally

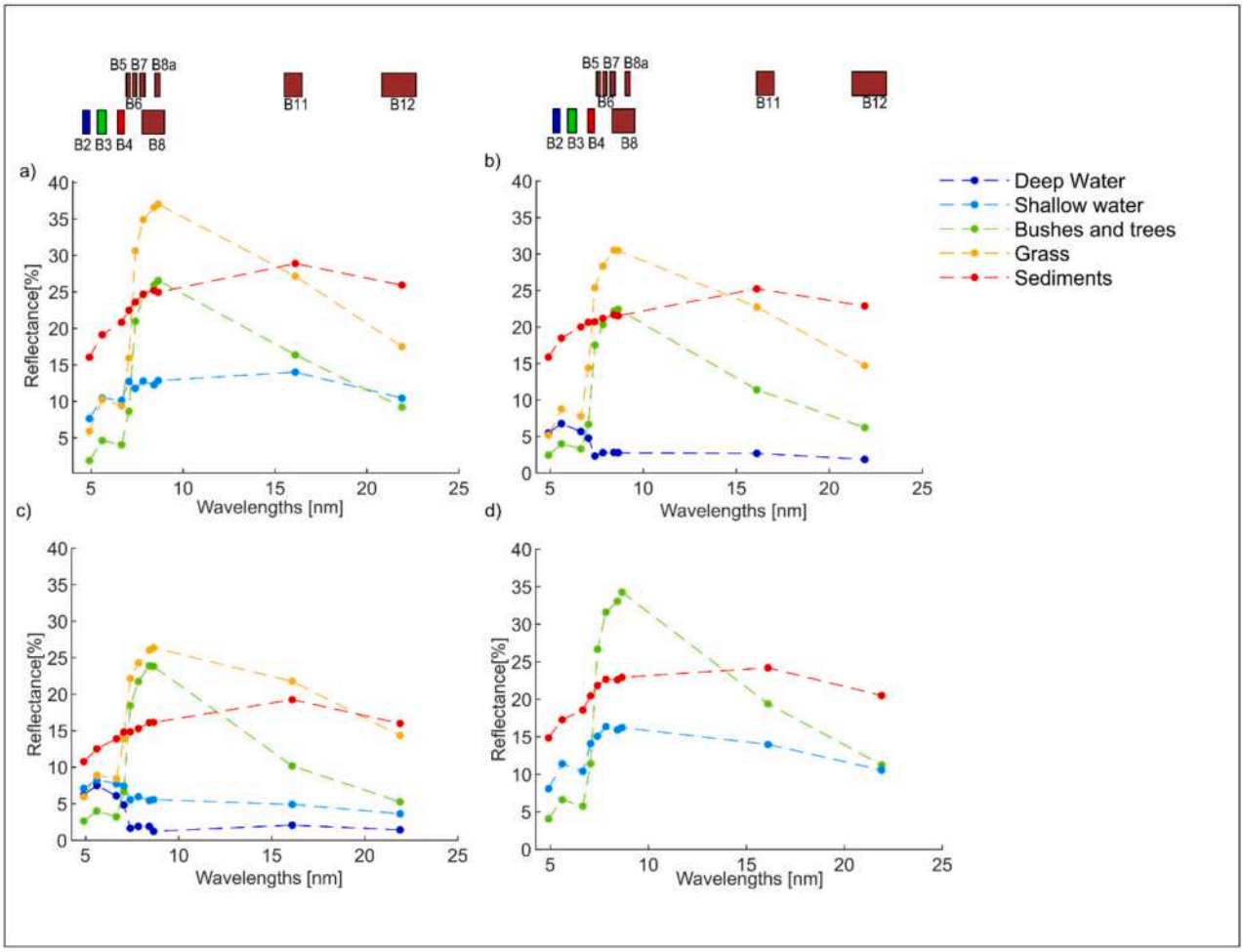

Fig. 4. A) spectral signature of 12 june 2019 where the google earth pro image was used as reference for classification; b) spectral signature of 6 february 2021 where fci and geolocated pictures were used for classification; c) spectral signature of 13 december 2021 where the orthophoto obtained by uav data was used for classification; d) spectral signature of 11 july 2022 where the orthophoto obtained by uav data was used for classification.

absorbed, giving place to spectral signature shapes like the ones shown in Fig. 4b and 4c. In contrast, as the water depth decreases, the reflectance values increase, mainly in the NIR and SWIR wavelengths. Specifically, the reflectance curves of the water extracted from the June 2019 and July 2022 images (Fig. 4a and 4d), both corresponding to a shallow water condition (≈0.50 m), show higher reflectance values in the infrared wavelengths than the spectral curve of the water extracted on 13th December 2021 (Fig. 4b). This can be due to the fact that the reflectance values of the shallow water bodies are influenced by the contribution of the bed reflection. Furthermore, it can be observed that the reflectance curve of the water extracted from the July 2022 image (Fig. 4d) shows higher values than the spectral curve of the water extracted in June 2019 (Fig. 4a) in all selected bands. On these two dates, the monitored reach was characterized by very different flow status: in June 2019, the reach had a continuous flow, whereas in July 2022, the reach was in a dry phase, characterized by an upstream sub-reach with water presence and a completely dry downstream sub-reach.

The high variability of the water spectral signature makes the identification of submerged areas by solely using water index-based classification methods more complex. In the studied river, the contribution from snow melt is negligible; the discharge mainly correlates with rainfall events and, hence, with a specific season of the year. Indeed, the catchment is typically affected by more water during the rainy season (autumn–winter) and by less water during the dry period (spring-summer). In order to be able to reliably distinguish these two different scenarios in the segmentation algorithm, we considered the spectral signature of high-depth water during the rainy period from November to April, and the spectral signature of shallow water during the rest of the year.

4.2. *Segmentation and classification*

As reference spectral signature, we selected the spectral signatures of shallow water, sediments and grass extracted from the June 2019 acquisition (cf. Fig. 4a) and the spectral signature of deep water from the December 2021 (cf. Fig. 4c). Classification results are, then, quantitatively validated on the remaining acquisitions, reported in Table 1. Fig. 5 shows a comparison between the results of the proposed MD method, the water mask extracted using the NDWI-based threshold method and the FCI. As already mentioned, the results of the MD method reported in Fig. 5 were obtained using the spectral signatures of shallow water, sediments and grass extracted from the June 2019 acquisition as reference spectral signatures (cf. Fig. 4a). For the deep water the reference spectral signature of the 13 December 2021 was used (cf. Fig. 4c). The MD method is able to correctly classify sediments, vegetation, wet channels and water ponds equal or larger than 10 m. Conversely, Fig. 5 (a3) shows that the MD method is unable to correctly classify the two small river channels with dimensions comparable to the pixel resolution, highlighted in the black box in Fig. 5(a1). This limitation is caused by the spatial resolution of the S2 data rather than the MD method itself. In Fig. 5, it can be observed that the MD method is able to classify the presence of water more accurately than NDWI during the summer

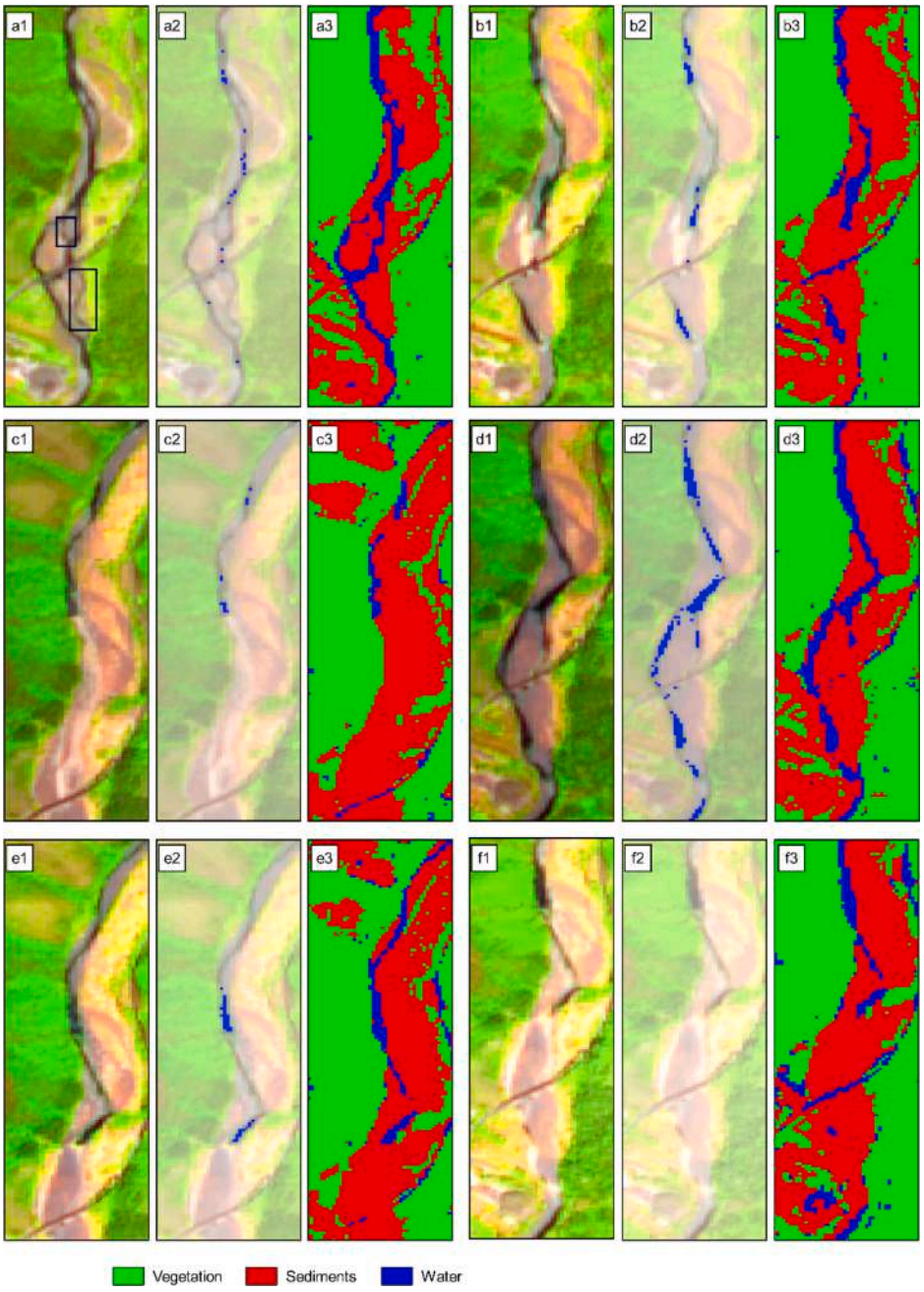

Fig. 5. Dry season: (a_1) FCI extracted by S2 acquisition of 12 June 2019, (a_2) NDWI overlapped with FCI, (a_3) classification map extracted from the MD method; (b_1) FCI extracted by S2 acquisition of 26 June 2020, (b_2) NDWI overlapped with FCI, (b_3) classification map extracted from the MD method; (c_1) FCI extracted by S2 acquisition of 26 July 2020, (c_2) NDWI overlapped with FCI, (c_3) classification map extracted from the MD method; (d_1) FCI extracted by S2 acquisition of 11 June 2022, (d_2) NDWI overlapped with FCI, (d_3) classification map extracted from the MD method; (e_1) FCI extracted by S2 acquisition of 16 July 2022, (e_2) NDWI overlapped with FCI, (e_3) classification map extracted from the MD method; (f_1) FCI extracted by S2 acquisition of 14 September 2022, (f_2) NDWI overlapped with FCI, (f_3) classification map extracted from the MD method.

period, when the water depth is very low. This represents a major advantage of the proposed MD method.

Fig. 6 shows images acquired in autumn, winter and early spring, during which the wet channel has higher water depth than in the summer season. In this case, due to the deep-water spectral signature (Fig. 4b and 4c) the classification based on NDWI threshold correctly classifies the presence of water. Instead, with the MD method, which uses the shallow water spectral signature as the reference spectral signature, the sediment is misclassified as water, namely the presence of water is overestimated. This is due not only to the already discussed change in shape of the spectral signature but also to the fact that sediments are typically wet during the rainy period and, therefore, are characterized by a lower spectral response in all bands. In these situations, the reflectance of the sediments is closer to the shallow water spectral signature and, consequently, they are misclassified as water. Conversely, as shown in the fourth column of the panel plot of Fig. 6, when in the MD method we consider the spectral signature of deep water instead of the spectral signature of shallow water, the results for water classification are better compared to the NDWI-based method. In this case, it is noteworthy that also the sediment and vegetation class is reliably classified in the active channel, which is unfeasible by using the classical NDWI-based approach.

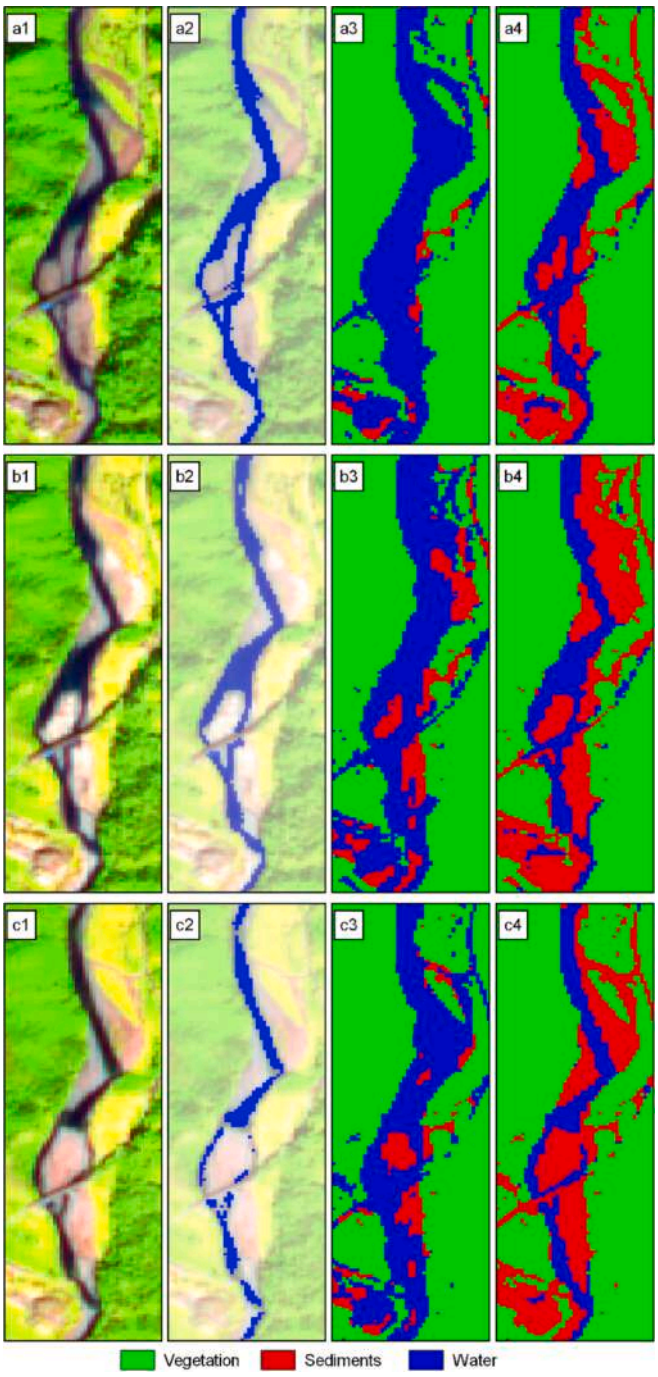

Fig. 6. Wet season: (a_1) FCI extracted by S2 acquisition of 13 December 2020, (a_2) NDWI overlapped with FCI, (a_3) classification map extracted from the MD method using the spectral signature of shallow water, (a_4) classification map extracted from the MD method using the spectral signature of deep water; (b_1) FCI extracted by S2 acquisition of 6 February 2021, (b_2) NDWI overlapped with FCI, (b_3) classification map extracted from the MD method using the spectral signature of shallow water, (b_4) classification map extracted from the MD method using the spectral signature of deep water; (c_1) FCI extracted by S2 acquisition of 13 March 2023, (c_2) NDWI overlapped with FCI, (c_3) classification map extracted from the MD method using the spectral signature of shallow water, (c_4) classification map extracted from the MD method using the spectral signature of deep water.

Tables 2 and 3 show the performance metrics resulting from the quantitative approach described in Sect. 3.3. As already mentioned we performed two tests. Test 1 compares the MD classifications with manual classification over the acquisition of July 2022 and February 2021. In the results reported in Table 2, a very good performance for all the considered metrics is shown. This striking result is also made possible thanks to the fact that the polygons, identified in the reference image, are fully representative of the different classes. In particular, we found good performances in distinguishing the vegetation class both in the July and February images. Nonetheless, in July some minor errors are observed in the classification of sediments and water classes. As already mentioned, it should be noted that the recognition of these two classes is challenging because the distance of the reference spectral signatures is quite small (see Fig. 4a e 4d).

Table 3 lists the performances obtained by Test 2 by comparing the MD and the NDWI results with the ground truth, given by the wet channel masks manually identified on the VHR images. Table 3 showed that for the summer dates (July and June) when water depth is lower, the recall performance is significantly higher by using the proposed MD method than the NDWI method. For these dates, the number of true positives is much higher for the case of the MD method than for the NDWI method, which, as also shown in Fig. 5, often fails to identify the presence of water during the summer season. On the other hand, it is worth noting that the recall values for the MD method never exceed 0.8, as the MD method is unable to identify wet channels with width smaller than 10 m (cf. Fig. 5a1,a2,a3). Moreover, it can be noticed that the precision of the NDWI method is systematically higher than the one of the MD method. However, this is because the NDWI method underestimates the water class, and this results in a low number of false positive. The reason of this discrepancy is that the proposed MD method uses several bands and, some of them have the lower resolution of 20 m (compared to the 10 m resolution of the other bands). Hence, a non-perfect alignment occurs between the water masks extracted by the 20-m spatial resolution images and the reference water mask, manually identified on the VHR images (cf. Fig. 7c). Conversely, the NDWI method is less affected by this misalignment because it only uses the 10-m spatial resolution bands (i.e., green and NIR). Furthermore, it is worth remarking that for the NDWI-based method the precision is higher than the MD method, but it fails to identify a large number of water pixels (false negative errors), which represents a major flaw of the method for applications on non-perennial rivers. For the summer acquisitions, the higher values of the F1 score further corroborate that the MD method performs significantly better than the NDWI method. For the case of images acquired in December, corresponding to higher water depths, the Recall metrics of the MD method is still higher than the value corresponding to the classical NDWI method. However, the Precision and, to a lesser extent, also the F1 score are higher for the case of the NDWI method. These confirm the acceptable performance of the classical NDWI method when the water depth is sufficiently high. Nonetheless, it should be remarked that, while the NDWI method sometimes exhibits false negative errors, the MD method is found to give an output for a certain number of false positive pixels. This discrepancy is once again due to the non-perfect alignment of the water mask by the MD method with the one by the VHR reference image (cf. Fig. 7c), but could be partially attributable also to occasional misclassification errors between

Table 2
Performance metrics on the considered polygons as ground truth.

Dates	Classes	Recall	Precision	F1-score	Overall Accuracy
11 July 2022	Sediments	0.916	0.943	0.930	
	Vegetation	1	1	1	0.960
	Water	0.966	0.950	0.958	
6 February 2021	Sediments	1	1	1	1
	Vegetation	1	1	1	
	Water	1	1	1	

Table 3
Comparison of the MD method and the NDWI-based method considering the manually extracted wet channel as ground truth.

Dates	Classes	Methods	Recall	Precision	F1-score
11 July 2022	W/NW	NDWI	0.406	0.922	0.564
		MD	0.786	0.641	0.706
13 December 2021	W/NW	NDWI	0.835	0.890	0.861
		MD	0.962	0.621	0.755
12 June 2019	W/NW	NDWI	0.017	1	0.034
		MD	0.659	0.590	0.623

wet sediments and water. To make the above argumentations clearer, in Fig. 7 we reported a further comparison of the water mask extracted by the MD method and the one manually obtained through naked-eye inspection of the orthophoto (by UAV data). From Fig. 7c it is clear that the water masks are slightly shifted. As explained above, this misalignment is essentially due to the different spatial resolutions of the 20 m bands employed by the MD method. Nonetheless, the substantial agreement between Fig. 7a and 7b confirms that the MD method succeeds in classifying the wet channel with reasonably good accuracy. However, the limitation related to the relatively low spatial resolution of the satellite data has to be considered: in fact, as it can be seen from Fig. 6, the MD method is unable to correctly identify wet channels narrower than ≈7 m (cf. also Fig. 7b in red box).

4.3. *Estimation of the duration of the dry bed period*

Knowledge about the river flow regime is essential to support river management and to preserve the related ecosystem services. In this section the water masks, previously extracted by the proposed MD method, are employed to estimate the dry bed periods of the monitored reaches. We found that the M1 reach, which is located in the upstream position, was never affected by totally dry periods: namely, continuous water lines or isolated ponds were observed in M1 throughout the entire observation period. Conversely, the downstream tract, M2, was found to be systematically affected by dry periods. Fig. 8 shows the duration of the dry periods of the M2 reach over the different years. The duration of the dry bed condition typically begins in August and ends in early

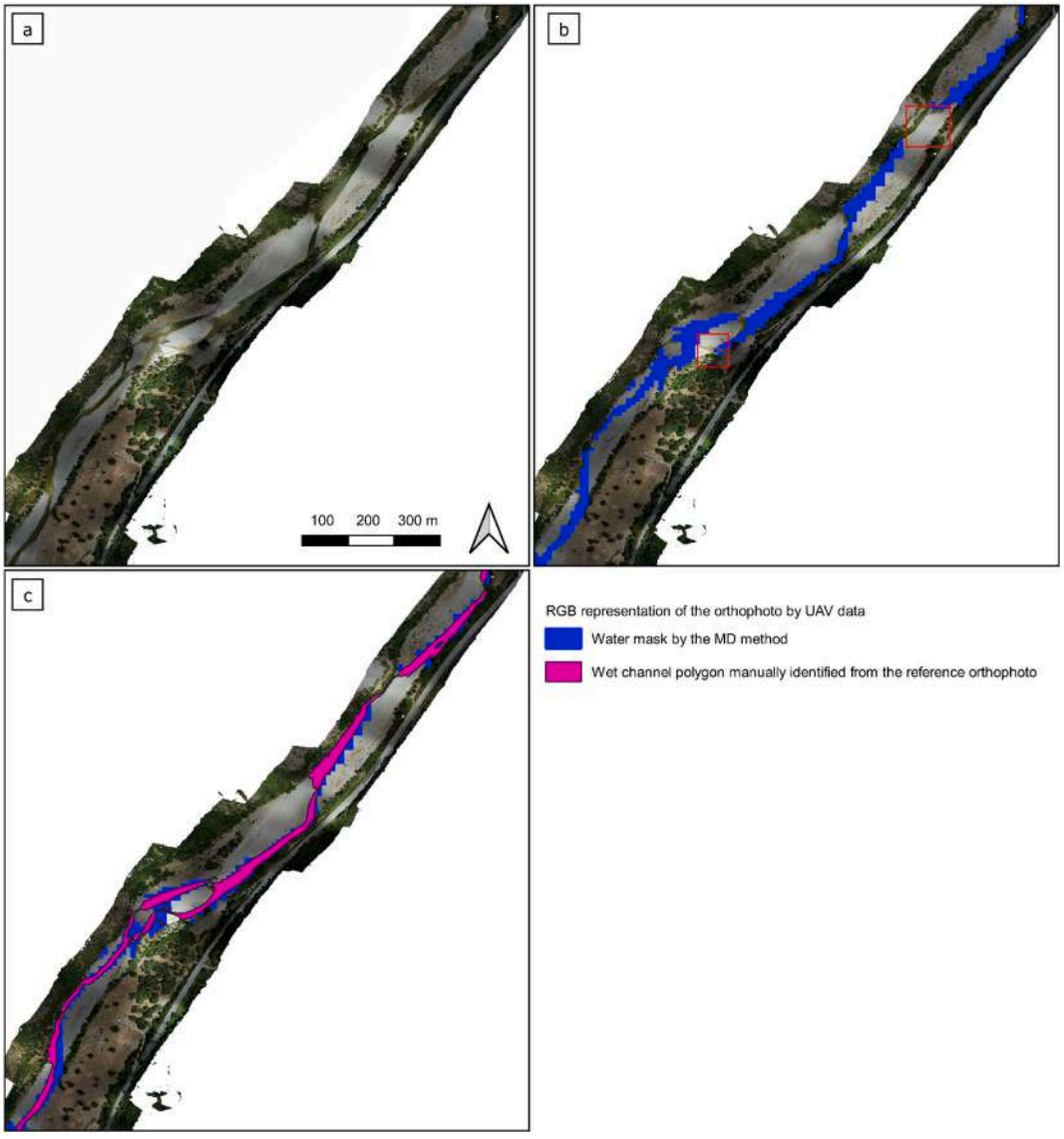

Fig. 7. (a) RGB representation of the orthophoto obtained by UAV data on 11 July 2022; (b) Water mask extracted by the MD method on the Sentinel-2 acquisition of 11 July 2022 superimposed on the orthophoto by UAV data and red boxes where the MD method does not identify the presence of water; (c) Overlay of the orthophoto, the water mask extracted by the MD method and the water mask manually identified from the reference orthophoto. (For interpretation of the references to colour in this figure legend, the reader is referred to the web version of this article.)

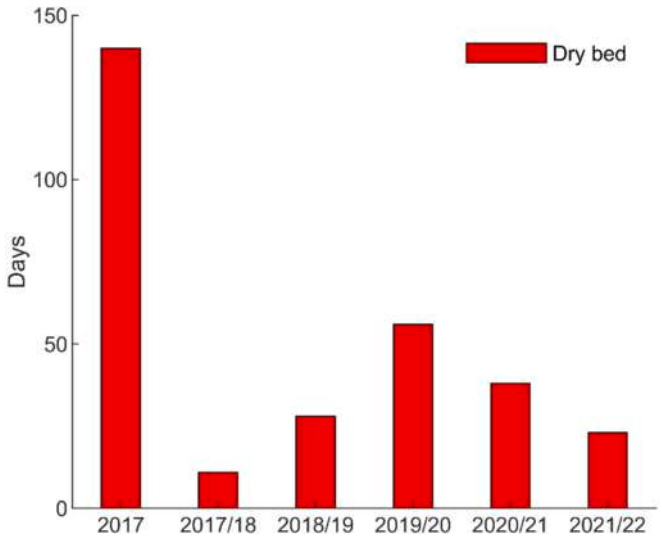

Fig. 8. Duration of the dry bed periods of the M2 reach over the different years.

October. The longest duration is found in 2017, when the M2 reach remained dry for a continuous time interval of ≈140 days (from June until the beginning of November). The results obtained in our analysis are consistent with those of Longobardi et al. (2021), who identified the year 2017 as the most critical year for drought in Campania. In 2017/2018 the dry bed condition only occurred in November 2017, which is attributable to an extension of the dry season of past summer. Conversely, it should be noted that no dry bed condition was observed in the next summer 2018. After the summer of 2017, a particularly prolonged dry period was observed in 2019/2020, lasting about 60 days. This was followed by the year 2020/2021, which experienced a dry period of approximately 40 days. The years 2018/2019 and 2021/2022, on the other hand, show dry periods lasting 30 and 25 days, respectively. In relation to the European reports (Toreti et al. 2022a,b) on the extreme drought of 2022, it is important to note that this event did not have significant effects in the Mingardo River basin. In fact, in 2022, while northern Italy suffered a severe drought and a significant drop in water levels, Campania experienced less critical situations. The dry phase generally begins in the sections close to the bridge (see Fig. 5b) and, then, extends upstream and downstream (see Fig. 5c and 5e). Typically, when the ponding phase starts along M2 reach, a continuous flowing phase persists in M1 reach. Presumably, this is due to the progressive descent of the water table in the underbed. As the dry period continues, the M2 reach transitions to a dry phase, while the M1 reach a ponding phase. The river morphology plays a crucial role in determining the presence of the ponds and the persistence of water in them. In fact, the M1 reach, characterized by a narrower riverbed with more variable morphology and partial vegetation cover, has longer ponding phases, while the wider M2 reach is characterized by less incised wet channels without vegetation cover and, therefore, requires shorter times for complete drying. Presumably, the longer water evaporation times along M1 reach could also result from the degree of confinement, which could lead to less radiation exposure. The prolonged drought conditions observed in the lower reaches of the river may be influenced by water withdrawals taking place in the upper part of the basin. These withdrawals can significantly reduce the flow of water downstream, leading to lowered water levels and extending prolonged dry periods.

Table 1S in the supplementary material presents a comparison between the classification obtained using the MD method and the water level measurements recorded at the hydrometric station located downstream of reach M2. It is observed that, for the dry images, the water level ranges between 2.54 m a.s.l. and 2.65 m a.s.l., whereas for the wet condition, the level ranges between 2.58 m a.s.l. and 3.15 m a.s.l..

5. Discussion

While there are a few simple index-based techniques in the literature for extracting water surfaces from multispectral sensors (e.g. the methods based on the NDWI, MNDWI and NDVI indices), mapping and monitoring the water presence along non-perennial rivers is still a big challenge, especially for narrow rivers and when the flow becomes shallow. Our results evidenced that index-based methods significantly underestimate the presence of water, if the water depth is small (order of ≈10 cm). The main reason for this shortcoming is related to the high variation in shape and magnitude of the spectral signature, as the water depth changes (cf. Fig. 4). Specifically, the increase of the near-infrared reflectance response, with decreasing water depth, makes it particularly difficult to exploit methods based on indices, where the principal component is typically the infrared band. In fact, the results shown in Figs. 5 and 6 demonstrate that NDWI is only able to classify the presence of water, when the water depth is high enough ($h > \approx 1$m). For the sake of brevity, we have only reported results based on the threshold of NDWI, because, according to Seaton et al. (2022) and Maswanganye et al. (2022), we found that methods based on different multispectral indices, such as the MNDWI or the NDVI, performed even worse in mapping water surfaces along non-perennial rivers.

Conversely, since the spectral signature of vegetation preserves its shape at different seasons, methods based on multispectral indices may be fruitfully used to distinguish densely vegetated from unvegetated or lightly vegetated areas (grass). In order to more reliably distinguish the water class from the other classes, we proposed a novel method, which fully exploits the various bands of the spectral signature and works by finding the minimum distance between the spectral signature (using 10 m and 20 m bands of S2) of any given pixel ($\mathbf{x}$) and the reference spectral signatures, corresponding to the different classes (water, sediment and grass). The MD method was implemented by using the spectral signatures for shallow water, sediment and grass taken in June; and for deep water an additional reference spectral signatures taken in December, namely in the wet season. In summary, for the application of the MD algorithm we use the same spectral signatures both in winter and in summer for sediment and grass, while for water we distinguish between a “shallow water” signature for the summer period and a “deep water” signature for the winter period. The use of only two reference spectral signatures, which are representative of the dry and wet seasons, was found to be sufficient to capture the key features of the spectral behavior of the water class during the entire hydrological year.

It is worth underlining that the proposed MD method, compared to index-based methods, utilizes the full information of all S2 satellite acquisition bands and requires no threshold calibration. In this respect, it will be shown that considering the entire spectral signature through the proposed MD approach yields more robust estimations. Furthermore, in the study of non-perennial rivers, the MD method allows for the classification of three classes (water, sediment and grass), different from threshold methods based on the use of a single index that usually are able to identify the sole water class. Yet, to our knowledge, a specific index has not yet been developed for sediment extraction.

The overall accuracy obtained from the numerical comparisons (Test 1), shown in Table 2, is always above 0.9 for all metrics (recall, precision and F1 score). We verified that similar results are obtained using the July spectral signature, for shallow water, grass and sediment, and the February spectral signature, for deep water, as reference spectral signatures. This is also highlighted by the lofty performance shown in Table 2, which reports the performance of the classification tested on the polygons obtained for the construction of the spectral signatures not used as a reference. Conversely, it was found that the NDWI method is only able to correctly identify water when the non-perennial river is in a clearly flowing phase with high water depths (cf. Fig. 6), while it systematically fails when water levels are low or isolated water ponds are present (cf. Fig. 5). This shortcoming of the NDWI method would result in a huge overestimation of the dry bed duration in the monitored

reaches. The numerical assessment, performed with Test 2, shows that for summer acquisitions, the Recall is higher for the MD method than for the NDWI, while the Precision is slightly lower. The MD method has a relatively lower precision due to a non-perfect alignment between the mask extracted by the method on the Sentinel-2 data and the mask obtained from the polygons identified on the VHR images (Fig. 7c), which leads to a shift between false-positive and true-positive pixels. Overall, for summer acquisition, the F1 score of the MD method is higher than that of the classical NDWI method. For the acquisition of December, slightly better performances are observed with the NDWI method compared to the MD method. This is probably caused by the fact that the proposed MD method is less reliable when wet sediments are present in the active channel. This result is not surprising considering that the NDWI method is specifically designed for working in these water conditions (McFeeters et al., 1996). Namely, this work confirms that water indices, such as the NDWI or MNDWI, can be suitably exploited to identify the water presence along rivers with high water depths, as recently reported also by Seaton et al. (2020) and Maswanganye et al. (2022a,b) , 2022b). In Fig. 5b2 and Fig. 5e2, in fact, the index is found to be able to correctly identify the presence of water, in correspondence with deeper pools. Instead, as shown in Fig. 5, the MD method is found to deliver significantly better results, when dealing with shallow water/dry conditions in non-perennial rivers. This makes it possible to extract more reliable water masks that can be used to estimate the duration of dry periods and to monitor hydro-morphological changes in the non-perennial rivers over time.

Compared to traditional measurement instruments, the MD method offers significant advantages in assessing hydrological regimes, particularly in identifying the dry bed season and estimating its duration. The hydrometer located downstream of reach M2, in fact, records levels between 2.54 m a.s.l. and 2.65 m a.s.l. when the river is dry and levels between 2.58 m a.s.l. and 3.15 m a.s.l. in wet conditions. It is therefore very disputable to set a level threshold to distinguish wet and dry conditions. Traditional hydrometric measurement systems reflect what occurs at the specific measurement point and are affected by river dynamics such as planimetric and elevation changes of the wet channel. This has little significant effect in flood stage measurement but may give misleading information when low levels are to be measured. In addition, it is worth noting that the hydrometric level at a specific point in the riverbed is not representative of the flow conditions at the river reach scale.

Therefore, satellite imagery provides crucial data for the understanding of hydrological dynamics of non-perennial rivers with the limitation that only rivers wider than 40 m and without vegetation cover can be monitored with currently available methods.

Based on the method proposed by Cavallo et al. (2022b), the MD method gives a result similar to the estimation of flow status duration. Thus, the important advantage introduced by the MD method is that an automatic classification of water, sediment and grass classes allows large-scale analysis. Furthermore, its application may yield coarse (interpolated) estimations when the time interval between two consecutive cloud-free images is long. However, it is noteworthy that generally during the dry periods, which is of interest for our analysis, the frequency of cloud cover is low and, thus, this problem is less relevant than in other applications. The dataset of flow status obtained by the MD method can be utilized to calibrate hydrologic models suitable for making predictions on a daily basis, as shown by Cavallo et al. (2022b). However, in that previous work, the analysis was only limited to the detection of presence and absence of water. The proposed MD method can be easily implemented for other case studies. The reference spectral signatures can be easily constructed for the specific case study with the help of the FCI or high-resolution images readily available on the internet and, as a clear advantage over pre-existent index-based methods, it is not required to calibrate any *ad-hoc* threshold. A limitation of the proposed approach is represented by the relatively low spatial resolution of the S2 satellite data that hinders the ability of the MD method to correctly identify wet channels with a width comparable with the pixel resolution (10 m) or smaller. We expect that this limitation of the satellite sensor may be overcome in the near future, as soon as satellite data are expanded to higher resolutions. The method presented in this paper can be applied to non-perennial rivers with active channel widths greater than 40 m and characterized by a Mediterranean-type climate.

The estimation of dry-bed duration and the water masks extracted from satellites provide a valuable tool to support further research efforts in the field of river hydrology, especially for better understanding the link between meteorological drought and the related river drought, as well as to the groundwater-surface water interactions. Moreover, the proposed approach may help to better assess the effects of water abstractions and the habitat availability for water-related species and, hence, may lead to a more conscious and sustainable management of non-perennial rivers.

6. Conclusion

In recent years, the scientific community has become increasingly interested in the hydrological regime of non-perennial rivers. The high spatial and temporal variability of river flow that characterizes such rivers cannot be fully captured with traditional gauging stations or from field observations. Sentinel-2 satellite data may provide a comprehensive view of the spatio-temporal variability of stream flow presence along reaches with an average active channel width larger than 40 m. To the best of our knowledge, the state-of-the-art methods to monitor non-perennial rivers use thresholds on multispectral indices (such as NDWI or MNDWI) that fail for the case of low water depths. To overcome such limitations, this paper proposes a new promising methodology that used the entire spectral signature of 10 m and 20 m Sentinel-2 bands to automatically identify three land cover classes (water, sediments and grass) within the active channel and, hence, to reliably estimate the dry bed duration and, therefore, flow intermittency. In particular, the proposed MD method is able to correctly identify water presence in different soil moisture condition. A major advantage of the proposed MD approach is that it does not require the calibration of any threshold value and, hence, is expected to yield robust estimations regardless of changes in the brightness condition of the scene. Water masks extracted from Sentinel-2 by the MD method can be fruitfully used to detect the presence of water along non-perennial rivers with an average temporal frequency of about 15 days during the wet season and 10 days during the dry season. The method is completely automatic and generalizable to any multispectral data with the necessary precautions. In future work, we intend to incorporate additional satellite data with spatial resolution better than 10 m in order to include the analysis of the wet channels with width smaller than 10 m.

Author contributions

Carmela Cavallo: Conceptualization, Data curation, Formal analysis, Methodology, Investigation, Software, Validation, Writing – original draft, Writing – review & editing, Visualization. **Luca Sarno:** Writing – review & editing, Visualization, Supervision. **Maria Nicolina Papa:** Conceptualization, Writing – review & editing, Visualization. **Giovanni Negro:** Conceptualization, Visualization. **Paolo Vezza**: Conceptualization, Visualization, Supervision. **Giuseppe Ruello**: Visualization. **Massimiliano Gargiulo:** Methodology, Software, Writing – review & editing.

Role of the funding source

This research did not receive any specific grant from funding agencies in the public, commercial, or not-for-profit sectors.

CRediT authorship contribution statement

Carmela Cavallo: Conceptualization, Data curation, Formal analysis, Investigation, Methodology, Resources, Software, Supervision, Validation, Visualization, Writing – original draft, Writing – review &

editing. **Luca Sarno:** Supervision, Visualization, Writing – review & editing. **Maria Nicolina Papa:** Conceptualization, Supervision, Visualization, Writing – review & editing. **Giovanni Negro:** Conceptualization, Visualization. **Paolo Vezza:** Conceptualization, Supervision, Visualization. **Giuseppe Ruello:** Visualization. **Massimiliano Gargiulo:** Methodology, Software, Writing – review & editing.

Declaration of competing interest

The authors declare that they have no known competing financial interests or personal relationships that could have appeared to influence the work reported in this paper.

Appendix A. Supplementary data

Supplementary data to this article can be found online at https://doi.org/10.1016/j.jhydrol.2025.133416.

Data availability

Data will be made available on request.

References

Carbonneau, P.E., Belletti, B., Micotti, M., Lastoria, B., Casaioli, M., Mariani, S., Bizzi, S., 2020. UAV-based training for fully fuzzy classification of Sentinel-2 fluvial scenes. *Earth Surf. Proc. Land.* 45 (13), 3120–3140.

Cavallo, C., Nones, M., Papa, M.N., Gargiulo, M., Ruello, G., 2021. Monitoring the morphological evolution of a reach of the Italian Po River using multispectral satellite imagery and stage data. *Geocarto Int.* 1–23.

Cavallo, C., Papa, M.N., Gargiulo, M., Palau-Salvador, G., Vezza, P., Ruello, G., 2021. Continuous monitoring of the flooding dynamics in the Albufera Wetland (Spain) by Landsat-8 and Sentinel-2 datasets. *Remote Sens. (Basel)* 13 (17), 3525.

Cavallo, C., Papa, M.N., Negro, G., Gargiulo, M., Ruello, G., Vezza, P., 2022b. Exploiting Sentinel-2 dataset to assess flow intermittency in non-perennial rivers. *Sci. Rep.* 12 (1), 21756.

Commission of the European Communities., 2009. *WHITE PAPER: Adapting to climate change: Towards a* European framework for action. Commission of the European Communities.

Curran, P.J., 1983. Multispectral remote sensing for the estimation of green leaf area index. *Philosophical Transactions of the Royal Society of London. Series A, Mathematical and Physical. Sciences* 309 (1508), 257–270.

Datry, T., Larned, S.T., Tockner, K., 2014. Intermittent Rivers: A Challenge for Freshwater Ecology. *Bioscience* 64, 229–235.

De Girolamo, A.M., Bouraoui, F., Buffagni, A., Pappagallo, G., Lo Porto, A., 2017. Hydrology under climate change in a temporary river system: Potential impact on water balance and flow regime. *River Res. Appl.* 33 (7), 1219–1232.

Di Ciacca, A., Wilson, S., Kang, J., Wöhling, T., 2023. Deriving transmission losses in ephemeral rivers using satellite imagery and machine learning. *Hydrol. Earth Syst. Sci.* 27 (3), 703–722.

EC, 2009a. White paper "Adapting to climate change: Towards a European framework for action"; [COM(2009) 147 final].

EC, 2009b. Common implementation strategy for the Water Framework Directive (2000/60/EC). Guidance document N. 24. River basin management in a changing climate. Technical report 2009–040. Brussels.

Faranda, D., Pascale, S., Bulut, B., 2023. Persistent anticyclonic conditions and climate change exacerbated the exceptional 2022 European-Mediterranean drought. *Environ. Res. Lett.*

Ferreira, L.G., Huete, A.R., 2004. Assessing the seasonal dynamics of the Brazilian Cerrado vegetation through the use of spectral vegetation indices. *Int. J. Remote Sens.* 25 (10), 1837–1860.

Feyisa, G.L., Meilby, H., Fensholt, R., Proud, S.R., 2014. Automated Water Extraction Index: A new technique for surface water mapping using Landsat imagery. Remote sensing of environment 140, 23–35.

Gao, S., Chen, M., Li, Z., Cook, S., Allen, D., Neeson, T., Hong, Y., 2021. Mapping dynamic non-perennial stream networks using high-resolution distributed hydrologic simulation: A case study in the upper blue river basin. *J. Hydrol.* 600, 126522.

Goutte, C., Gaussier, E., 2005. A probabilistic interpretation of precision, recall and F-score, with implication for evaluation. In Advances in Information Retrieval: 27th European Conference on IR Research, ECIR 2005, Santiago de Compostela, Spain, March 21–23, 2005. *Proceedings 27*. Springer, Berlin Heidelberg, pp. 345–359.

Gurnell, A.M., Rinaldi, M., Belletti, B., Bizzi, S., Blamauer, B., Braca, G., Ziliani, L., 2016. A multi-scale hierarchical framework for developing understanding of river behaviour to support river management. *Aquat. Sci.* 78, 1–16.

Holben, B.N., 1986. Characteristics of maximum-value composite images from temporal AVHRR data. *Int. J. Remote Sens.* 7 (11), 1417–1434.

Ishida, T., Ando, H., Fukuhara, M., 1991. Estimation of complex refractive index of soil particles and its dependence on soil chemical properties. *Remote Sens. Environ.* 38 (3), 173–182.

Longobardi, A., Boulariah, O., Villani, P., 2021. Assessment of centennial (1918–2019) drought features in the Campania region by historical in situ measurements (southern Italy). *Nat. Hazards Earth Syst. Sci.* 21 (7), 2181–2196.

Ma, S., Zhou, Y., Gowda, P.H., Dong, J., Zhang, G., Kakani, V.G., Jiang, W., 2019. Application of the water-related spectral reflectance indices: A review. *Ecol. Ind.* 98, 68–79.

Maswanganye, S.E., Dube, T., Jovanovic, N., Mazvimavi, D., 2022a. Use of multi-source remotely sensed data in monitoring the spatial distribution of pools and pool dynamics along non-perennial rivers in semi-arid environments. South Africa. *Geocarto International* 1–20.

Maswanganye, S.E., Dube, T., Jovanovic, N., Kapangaziwiri, E., Mazvimavi, D., 2022b. Using the water balance approach to understand pool dynamics along non-perennial rivers in the semi-arid areas of South Africa. *J. Hydrol.: Reg. Stud.* 44, 101244.

McFeeters, S.K., 1996. The use of the Normalized Difference Water Index (NDWI) in the delineation of openwater features. *Int. J. Remote Sens.* 17 (7), 1425–1432.

Messager, M.L., Lehner, B., Cockburn, C., Lamouroux, N., Pella, H., Snelder, T., Datry, T., 2021. Global prevalence of non-perennial rivers and streams. *Nature* 594 (7863), 391–397.

Richards, J.A., Jia, X., 2006. *Interpretation of hyperspectral image data*. An Introduction, Remote Sensing Digital Image Analysis, pp. 359–388.

Rutkay, A.T.U.N., Kalkan, K., Gürsoy, Ö., 2020. Determining the forest fire risk with Sentinel 2 images. *Turkish Journal of Geosciences* 1 (1), 22–26.

Seaton, D., Dube, T., Mazvimavi, D., 2020. Use of multi-temporal satellite data for monitoring pool surface areas occurring in non-perennial rivers in semi-arid environments of the Western Cape, South Africa. *ISPRS J. Photogramm. Remote Sens.* 167, 375–384.

Shanafield, M., Bourke, S.A., Zimmer, M.A., Costigan, K.H., 2021. An overview of the hydrology of non-perennial rivers and streams. *Wiley Interdiscip. Rev. Water* 8 (2), e1504.

Toreti, A., Bavera, D., Avanzi, F., Cammalleri, C., DE, F. M., DE, J. A., ... & VAN, D., 2022a. Drought in northern Italy-March 2022: GDO analytical report.

Toreti, A., Bavera, D., Acosta Navarro, J., Cammalleri, C., de Jager, A., Di Ciollo, C., Spinoni, J., 2022b. Drought in Europe august 2022. Publications Office of the European Union, Luxembourg.

Wang, Z., Vivoni, E.R., 2022. Detecting Streamflow in Dryland Rivers Using CubeSats. Geophys. Res. Lett. 49 (15).

Xu, H., 2006. Modification of normalised difference water index (NDWI) to enhance open water features in remotely sensed imagery. Int. J. Remote Sens. 27 (14), 3025–3033.

Zimmer, M.A., McGlynn, B.L., 2017. Bidirectional stream–groundwater flow in response to ephemeral and intermittent streamflow and groundwater seasonality. *Hydrol. Process.* 31 (22), 3871–3880.

Zimmer, M.A., Kaiser, K.E., Blaszczak, J.R., Zipper, S.C., Hammond, J.C., Fritz, K.M., Allen, D.C., 2020. Zero or not? Causes and consequences of zero-flow stream gage readings. *Wiley Interdiscip. Rev. Water* 7 (3), e1436.